

# Induced-charge electrophoresis near an insulating wall

Mustafa Sabri Kilic<sup>1</sup> and Martin Z. Bazant<sup>1,2</sup>

<sup>1</sup> *Department of Mathematics, Massachusetts Institute of Technology, Cambridge, MA 02139, USA and*

<sup>2</sup> *Physico-Chimie Théorique, Gulliver-CNRS, ESPCI, 10 rue Vauquelin, Paris 75005, France*

(Dated: November 20, 2018)

Induced-charge electrophoresis (ICEP) has mostly been analyzed for asymmetric particles in an infinite fluid, but channel walls in real systems further break symmetry and lead to dielectrophoresis (DEP) in local field gradients. Zhao and Bau (Langmuir, **23**, 2007, pp 4053) recently predicted that a metal (ideally polarizable) cylinder is repelled from an insulating wall in a DC field. We revisit this problem with an AC field and show that attraction to the wall sets in at high frequency and leads to an equilibrium distance, where DEP balances ICEP, although, in three dimensions, a metal sphere is repelled from the wall at all frequencies. This conclusion, however, does not apply to asymmetric particles. Consistent with the recent experiments of Gangwal et al. (arXiv:0708.2417), we show that a metal/insulator Janus particle is always attracted to the wall in an AC field. The Janus particle tends to move toward its insulating end, perpendicular to the field, but ICEP torque rotates this end toward the wall. Under some conditions, the theory predicts steady translation along the wall with an equilibrium tilt angle, as seen in experiments, although more detailed modeling of the contact region of overlapping double layers is required.

DRAFT

## I. INTRODUCTION

Most theoretical work on electrophoresis has focused on spherical particles moving in an infinite fluid in response to a uniform applied electric field [2, 17, 27, 35]. Of course, experiments always involve finite geometries, and in some cases walls play a crucial role in electrophoresis. The linear electrophoretic motion of symmetric (spherical or cylindrical) particles near insulating or dielectric walls [8, 12, 18, 19, 20, 28] and in bounded cavities or channels [6, 7, 13, 14, 15, 21, 22, 24, 37, 48] has been analyzed extensively. Depending on the geometry and the double-layer thickness, walls can either reduce or enhance the translational velocity, and the rotational velocity can be opposite to the rolling typical of sedimentation near a wall. The classical analysis for thin double layers assumes “force-free” motion driven by electro-osmotic slip alone, but recent work has shown that electrostatic forces can also be important near walls [16, 45]. Heterogeneous particles with non-uniform shape and/or zeta potential exhibit more complicated bulk motion [1, 9, 25, 26], which can also affect boundary interactions [42], especially if the particles are deformable, as in the case of chain-like biological molecules [31].

In this article, we focus on the effect of nonlinear induced-charge electro-osmotic (ICEO) flows at polarizable surfaces, which are finding many new applications in microfluidics and colloids [4, 39, 41]. The canonical example of quadrupolar ICEO flow around a polarizable particle, first described by Murtsovkin [10, 30], involves fluid drawn in along field axis and expelled radially in the equatorial plane in an AC or DC field. Broken symmetries in this problem can generally lead to hydrodynamic forces and motion induced-charge electrophoresis (ICEP), as well as electrical forces and mo-

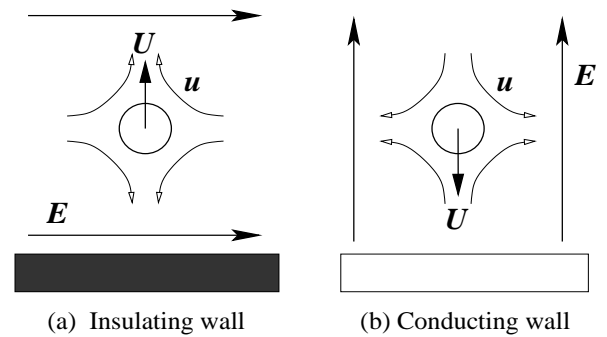


FIG. 1: Hydrodynamic forces on polarizable particles near (a) insulating and (b) unscreened conducting walls due to ICEO flows

tion by dielectrophoresis (DEP). Such phenomena have only been analyzed for isolated asymmetric particles in an infinite fluid [4, 40, 44] or in a dilute solution far from the walls [34, 36]. In contrast, experiments demonstrating translational ICEP motion have involved strong interactions with walls [11, 29], which remain to be explained.

As shown in Figure 1, it is easy to see that the quadrupolar ICEO flow around a polarizable particle typically causes attraction to unscreened conducting walls (perpendicular to the field) and repulsion from insulating walls (parallel to the field). The former effect of ICEP attraction to conducting walls has not yet been analyzed; it may play a role in colloidal self assembly on electrodes applying AC voltages [32, 33, 38, 43, 46]. This phenomenon is mainly understood in terms of electrohydrodynamic flows (what we would term “ICEO”) induced on the electrodes, not the particles (typically latex spheres), but ICEP could be important for more polarizable particles.

The latter effect of ICEP repulsion from insulating walls has recently been analyzed by Zhao and Bau [47] in the case

of a two-dimensional ideally polarizable cylinder in a DC field. However, this phenomenon has not yet been confirmed experimentally. On the contrary, Gangwal et al [11] have recently observed that metallo-dielectric Janus particles are attracted to a glass wall, while undergoing ICEP motion parallel to the wall and perpendicular to an applied AC field. It is not clear that the existing theory of ICEP can explain this surprising behavior.

The objective of this work is to analyze the motion of three-dimensional polarizable particles near insulating walls in AC fields. As summarized in section II, we employ the standard low-voltage model in the thin double-layer approximation, following many authors [3, 23, 39, 40, 44], including Zhao and Bau [47]. In section III, we first analyze ideally polarizable cylinders and spheres near a non-polarizable wall, which only experience forces perpendicular to the wall. In section IV we then study spherical metal/insulator Janus particles, which are half ideally polarizable and half non-polarizable. Due to their broken symmetry, the Janus particles also experience ICEP and DEP torques, which strongly affect their dynamics near the wall.

## II. MATHEMATICAL MODEL

### A. Low Voltage Theory

In this paper, we will consider either a cylindrical or a spherical particle of radius  $a$  in a semi-infinite electrolyte bounded by a plane. The distance between the center of the particle and the plane is denoted by  $h$ . In the absence of an applied electric field, we assume that the particle and the wall surfaces are uncharged. In addition, we will assume the electrolyte has a low Reynolds number, and impose Stokes equations. We will assume that the thin double layer approximation holds and the bulk electrolyte remains electroneutral, which is the case when the Debye length

$$\lambda_D = \sqrt{\frac{\epsilon kT}{2z^2 e^2 c_0}}$$

is much smaller than the characteristic length scale (in our case,  $a$ ). The Debye length typically ranges between 1 – 100nm, and colloidal particles are usually in the  $\mu$  range, therefore thin double layer approximation holds for most of the time.

Then the general equations consist of the Laplace's

$$\epsilon \nabla^2 \phi = 0$$

and Stokes equations

$$\begin{aligned} \eta \nabla^2 \mathbf{u} &= \nabla p \\ \nabla \cdot \mathbf{u} &= 0 \end{aligned} \quad (1)$$

where  $\phi$  is the electrostatic potential and  $\epsilon$  the permittivity,  $\eta$  the viscosity of the electrolyte,  $\mathbf{u}$  the velocity field and

$p$  the pressure. The wall boundary  $z = 0$  is an insulator, satisfying

$$\mathbf{n} \cdot \nabla \phi = 0$$

whereas the particle surface, being polarizable, acts as a capacitor in the thin double layer limit

$$\frac{dq}{dt} = (-\mathbf{n}) \cdot (-\kappa \nabla \phi)$$

with  $q$  being the surface charge density on the particle,  $\kappa$  the conductivity of the bulk electrolyte. Far away from the particle, an electric field

$$\nabla \phi \sim \mathbf{E}_\infty = E_\infty \hat{\mathbf{x}}, \quad |\mathbf{x}| \rightarrow \infty$$

is applied. In general, the magnitude  $E_\infty = E_\infty(t)$  may be time dependent.

The Stokes equations are supplied by the no-slip conditions on the wall and the Smoluchowski's electrokinetic slip formula on the particle

$$\mathbf{u} = \mathbf{u}_{slip} = \frac{\epsilon}{\eta} \zeta \nabla_s \phi$$

where  $\zeta$  is the potential difference between the surface and the bulk. Later, we will take into account the steric effects of ions and show how this formula needs to be modified. Lastly, we assume flow vanishes at the infinities.

So far, the equations are complete except for a constitutive relation between  $\zeta$  and  $q$ . The linear theory asserts that

$$q = -\frac{\epsilon}{\lambda_D} \zeta$$

although the complete problem is still nonlinear in this case because of the quadratic slip formula (5). In this paper, we will study only the linear theory, but the calculations can be repeated with (sometimes more accurate) nonlinear theories like that of Poisson-Boltzmann.

### B. Force and Torque on the Particle

Throughout this paper, we will assume that the particle is fixed and calculate the forces on the particle. For the case of a moving particle, the slip velocity needs to be modified to account for the motion of the particle surface.

The total force and torque on any volume of the fluid are conveniently given in terms of the stress tensor,  $\sigma$ , by

$$\mathbf{F} = \int_{\partial\Omega} \mathbf{n} \cdot \sigma dA \quad (2)$$

$$\mathbf{T} = \int_{\partial\Omega} \mathbf{r} \times (\mathbf{n} \cdot \sigma) dA \quad (3)$$

The stress tensor contains from electrical and viscous stresses on the fluid,  $\sigma = \sigma_M + \sigma_H$ , where

$$\sigma_M = \epsilon [\mathbf{E}\mathbf{E} - \frac{1}{2} E^2 \mathbf{I}]$$

$$\sigma_H = -p \mathbf{I} + \eta (\nabla \mathbf{u} + (\nabla \mathbf{u})^T)$$

are the Maxwell and hydrodynamic stress tensors, respectively.

### C. Particle Dynamics

In order to calculate the movement of a colloidal particle, we need to find a translational velocity  $\mathbf{U}$ , and a rotational velocity  $\mathbf{\Omega}$  such that the net force on the particle is zero, when the slip velocity is modified by taking into account the velocities  $\mathbf{U}$  and  $\mathbf{\Omega}$ . In other words, we are seeking  $\mathbf{U}$  and  $\mathbf{\Omega}$  such that the problem (1) with boundary condition

$$\mathbf{u} = \mathbf{u}_{slip} + \mathbf{U} + \mathbf{r} \times \mathbf{\Omega}$$

yields  $\mathbf{F} = \mathbf{0}$  and  $\mathbf{T} = \mathbf{0}$ .

Since Stokes problem is linear, there is a linear relationship between the translational and rotational motion of the particle and the resulting force and torque exerted on it by the fluid. Let us denote this relationship by

$$\begin{pmatrix} \mathbf{F} \\ \mathbf{T} \end{pmatrix} = \mathbf{M} \begin{pmatrix} \mathbf{U} \\ \mathbf{\Omega} \end{pmatrix}$$

The viscous hydrodynamic tensor  $M$  comes from solving for the Stokes flow around a particle moving with translational velocity  $\mathbf{U}$  and and rotational velocity  $\mathbf{\Omega}$ , assuming no slip on all particle and wall surfaces.

If we then solve the electrokinetic problem for a fixed particle in the applied field, we obtain the ICEO slip velocity  $\mathbf{u}_{slip}$  as well as the total (hydrodynamic + electrostatic) force  $\mathbf{F}_{slip}$  and torque  $\mathbf{T}_{slip}$  needed to hold the particle in place, thereby preventing ICEP and DEP motion.

Using these calculations and invoking linearity, the condition of zero total force and torque on the particle,  $\begin{pmatrix} \mathbf{F} \\ \mathbf{T} \end{pmatrix} + \begin{pmatrix} \mathbf{F}_{slip} \\ \mathbf{T}_{slip} \end{pmatrix} = 0$ , determines the motion of the particle

$$\begin{pmatrix} \mathbf{U} \\ \mathbf{\Omega} \end{pmatrix} = -\mathbf{M}^{-1} \begin{pmatrix} \mathbf{F}_{slip} \\ \mathbf{T}_{slip} \end{pmatrix} \quad (4)$$

The particle trajectory is then described by the solution to the differential equation

$$\frac{d\mathbf{x}}{dt} = \mathbf{U}$$

together with the equations for the particle's angular orientation.

This angular orientation does not matter for a full polarizable or insulating particle. For the Janus particle, we will argue that only the rotations about  $x$ -axis are important, thus we will focus on the dynamics of just a single angle. In this case, the equation of motion is simply

$$\frac{d\theta}{dt} = \Omega_x$$

### D. Nondimensional Equations

We nondimensionalize the variables by

$$\begin{aligned} \mathbf{x}' &= \frac{\mathbf{x}}{a}, & \phi' &= \frac{\phi}{E_\infty a}, & \zeta' &= \frac{\zeta}{E_\infty a} \\ q' &= \frac{\varepsilon E_\infty a}{\lambda_D} q \\ t' &= \left( \frac{\lambda_D a}{D} \right)^{-1} t, & t'' &= \left( \frac{\eta}{\varepsilon E_\infty^2} \right)^{-1} t \\ \mathbf{u}' &= \mathbf{u} \left( \frac{\varepsilon E_\infty^2 a}{\eta} \right)^{-1}, & p' &= \frac{p}{\varepsilon E_\infty^2} \end{aligned}$$

Note that there are two time scales in the problem,  $\tau' = \frac{\lambda_D a}{D}$ , the charging time, and  $\tau'' = \frac{\eta}{\varepsilon E_\infty^2}$ , the time scale for particle motion.

Plugging in the equations, we obtain (after dropping the primes except for  $t$ )

$$\begin{aligned} \nabla^2 \phi &= 0 \\ \nabla^2 \mathbf{u} &= \nabla p \\ \nabla \cdot \mathbf{u} &= 0 \end{aligned}$$

with the boundary conditions

$$\begin{aligned} \frac{dq}{dt'} &= \mathbf{n} \cdot \nabla \phi \\ \mathbf{u} &= \zeta \nabla_s \phi \end{aligned} \quad (5)$$

on the particle surface, where  $\zeta = \phi_{surface} - \phi_{bulk}$ , is the zeta potential. For a polarizable particle, we have  $\phi_{surface} = 0$  by symmetry, therefore we are left with  $\zeta = -\phi_{bulk} = -\phi$ .

In addition, we have

$$\nabla \phi \sim \hat{\mathbf{x}}, |\mathbf{x}| \rightarrow \infty$$

just as before, now with the dimensionless variables. The remaining equations are the no-slip boundary condition on the planar wall, and the requirement that the flow vanishes at infinities.

The constitutive relation between  $q$  and  $\zeta$  takes the simple form

$$\bar{q} = -\zeta = \phi$$

for the linear theory that we are going to analyze in this paper.

The dimensionless force and torque on the particle are given by the formulae (2) and (3), where the stress tensors are replaced by their dimensionless counterparts

$$\begin{aligned} \sigma_M &= \mathbf{E}\mathbf{E} - \frac{1}{2}E^2\mathbf{I} \\ \sigma_H &= -p\mathbf{I} + (\nabla\mathbf{u} + (\nabla\mathbf{u})^T) \end{aligned}$$

The force, angular momentum and stress tensors are scaled to

$$F_{ref} = \varepsilon E_\infty^2 a, \quad T_{ref} = \varepsilon E_\infty^2 a^2, \quad \sigma_{ref} = \varepsilon E_\infty^2$$

Finally, the particle motion will be governed by

$$\frac{d\mathbf{x}}{dt''} = \mathbf{U}, \quad \frac{d\theta}{dt''} = \Omega_x$$

## E. Simplifications

### 1. Steady Problems

If a DC voltage is applied, then the system reaches a steady state after a while and the time derivatives drop out. This is the case when Neumann boundary conditions are valid also on the cylinder or sphere. In that case

$$\begin{aligned} F_E &= \int_{\partial\Omega} (\mathbf{E}\mathbf{E} - \frac{1}{2}E^2\mathbf{I})\mathbf{n}dA \\ &= \int_{\partial\Omega} (\mathbf{E}\mathbf{E} \cdot \mathbf{n} - \frac{1}{2}E^2\mathbf{n})dA = -\frac{1}{2} \int_{\partial\Omega} E^2\mathbf{n}dA \end{aligned}$$

because  $\mathbf{E} \cdot \mathbf{n} = 0$  on the surface. As a consequence, the electrostatic torque induced on the particle is zero.

### 2. Symmetry

For the full cylinder problem, the electrostatic problem has an odd symmetry in  $x$ -direction, that is

$$\phi(x, z) = -\phi(-x, z)$$

and for the full sphere problem, it has an odd symmetry in  $x$ -direction and an even symmetry in  $y$ -direction:

$$\phi(x, y, z) = \phi(x, \pm y, z) = -\phi(-x, y, z)$$

As a result,  $E^2$  has even symmetry in  $x$  and  $y$ . Therefore, in the steady case, the electrostatic forces vanish in those directions, and there can only be a vertical force. In general time-dependent cases,  $E$  has an even symmetry in  $x$  and odd symmetry in  $y$ , and therefore the electrostatic force may not vanish in  $x$  direction.

As for the Stokes problem, a glance at the slip formula shows that the slip, just like the potential field, has an odd symmetry in both  $x$  and  $y$ , and therefore so does the flow field. Consequently, there are no hydrodynamic forces in those directions.

Needless to say, all these symmetry arguments disappear for the Janus particles.

## 3. AC fields

In the linear model we are considering, the time-periodic electrostatic forcing problem can be solved by letting

$$\phi = \text{Re}(\tilde{\phi}e^{i\omega t})$$

and solving for the complex potential  $\tilde{\phi}$  using the equations

$$\nabla^2 \tilde{\phi} = 0$$

with the boundary conditions

$$\begin{aligned} n \cdot \nabla \tilde{\phi} &= i\omega \tilde{\phi} \quad (\text{polarizable}) \\ n \cdot \nabla \tilde{\phi} &= 0 \quad (\text{insulator}) \\ \tilde{\phi} &= -E_\infty x \quad (\text{at infinity}) \end{aligned}$$

In the high frequency limit, the electrostatic problem approaches to the solution of the dirichlet problem, that is, the first boundary condition is replaced by

$$\tilde{\phi} = 0 \quad (\text{polarizable}) \quad (6)$$

This is because  $\tilde{\phi} = n \cdot \nabla \tilde{\phi} / i\omega \approx 0$ . Physically, this means that the double layers do not have enough time to charge when the forcing frequency is too high.

Note that in cases of AC fields below, it is the field amplitude  $E_0$  that enters into the scalings above, and the  $U$  is the time-averaged velocity.

Once the electrostatic potential is calculated, the time-averaged slip velocity can be obtained by the formula

$$\mathbf{u}_s = \frac{1}{2} \text{Re}[\tilde{\zeta} \tilde{E}_{//}^*] \quad (7)$$

where  $\tilde{\zeta}$  is the (complex) surface zeta potential, which is equal to  $-\tilde{\phi}$  in the linear theory, and  $\tilde{E}_{//}^*$  is the complex conjugate of the tangential component of  $\tilde{E} = \nabla \tilde{\phi}$ , the complex electric field.

In the DC limit as  $\omega \rightarrow 0$ , the imaginary parts of the solutions go to zero, and we are left with  $\mathbf{u}_s = \frac{1}{2}\zeta E_{//}$ , which is the standard Smoluchowski's formula with a factor of 1/2.

## F. Numerical Methods

We have solved the equations using the finite element software COMSOL for various geometries which have been approximated by the cylindrical or spherical colloidal particle being enclosed by a finite rectangle. The equations are first converted to their weak forms, and entered into the general weak PDE module of COMSOL. None of the COMSOLs special modules are used.

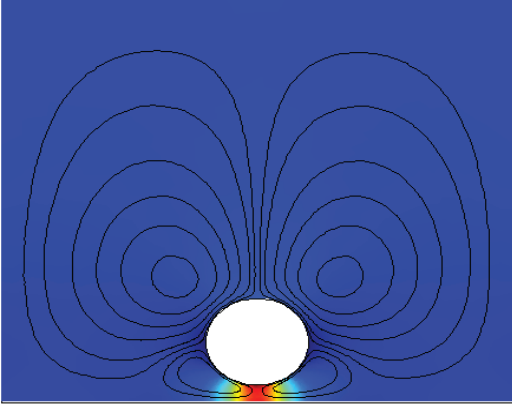


FIG. 2: Streamlines to the Stokes flow problem for a cylinder near a wall. The surface color indicates the pressure. In this case, the increased pressure between the wall and the cylinder leads to repulsion away from the wall.

For linear and nonlinear models alike, the computational efficiency is improved by first solving the electrostatic problem, and then the hydrodynamic problem. In time dependent cases, the fluid slip can be averaged and the Stokes problem is solved only once using this averaged slip.

For reasons of completeness and easy reference, here we list the weak forms of the equations solved. This system of equations are converted to weak form by multiplying by corresponding test functions and integrating over the spatial domain.

The electrical problem turns into

$$\begin{aligned} 0 &= - \int_{\Omega} \hat{\phi} \nabla^2 \phi \, d\mathbf{r} = \int_{\Omega} \nabla \hat{\phi} \nabla \phi \, d\mathbf{r} + \int_{\partial\Omega} \hat{\phi} (\mathbf{n} \cdot \nabla \phi) \, ds \\ &= \int_{\Omega} \nabla \hat{\phi} \nabla \phi \, d\mathbf{r} + \int_{\partial\Omega} \hat{\phi} \partial_t q \, d\mathbf{r} \end{aligned}$$

which is satisfied for all test functions  $\hat{\phi}$ . The boundary condition for  $\phi$  is imposed in the form

$$0 = \int \hat{q} (V_{\text{col}} - \phi - \zeta) \, d\mathbf{r}$$

to be satisfied for all test functions  $\hat{q}$ .

The weak form for the stokes flow is similarly obtained as

$$\begin{aligned} 0 &= - \int_{\Omega} [\hat{\mathbf{u}} \cdot (\nabla \cdot \boldsymbol{\sigma})] \, d\mathbf{r} + \hat{p} \int_{\Omega} \nabla \cdot \mathbf{u} \, d\mathbf{r} \\ &= - \int_{\Omega} [\nabla \hat{\mathbf{u}} : \boldsymbol{\sigma} - \hat{p} \nabla \cdot \mathbf{u}] \, d\mathbf{r} + \int_{\partial\Omega} \hat{\mathbf{u}} \cdot (\mathbf{n} \cdot \boldsymbol{\sigma}) \, ds \end{aligned}$$

Since we do not have a simple expression for  $\mathbf{n} \cdot \boldsymbol{\sigma}$ , it is best to introduce the new variable (Lagrangian multiplier)  $\mathbf{f} = \mathbf{n} \cdot \boldsymbol{\sigma}$ .

This is also convenient for calculation of hydrodynamic forces at the surface. Then we obtain

$$0 = - \int_{\Omega} [\nabla \hat{\mathbf{u}} : \boldsymbol{\sigma} - \hat{p} \nabla \cdot \mathbf{u}] \, d\mathbf{r} + \int_{\partial\Omega} [\hat{\mathbf{u}} \cdot \mathbf{f} + \hat{\mathbf{f}} \cdot (\mathbf{u} - \mathbf{u}_s)] \, ds$$

### III. ISOTROPIC PARTICLES NEAR A WALL

#### A. Cylinder in a DC Field

For isotropic particles near a wall, by symmetry,  $\phi_{\text{cylinder}} = 0$ , therefore  $\zeta = -\phi$ . Moreover, there is no net horizontal force exerted on the particle, so the only forces of interest is in the vertical direction. Another consequence of symmetry is the absence of net torque on the cylinder.

The DC cylinder problem has been solved analytically by Zhao and Bau [47] in the linear case in bipolar coordinates. The mapping between the bipolar and the Cartesian coordinates is given by

$$x = \frac{c \sin \beta}{\cosh \alpha - \cos \beta}, \quad y = \frac{c \sinh \alpha}{\cosh \alpha - \cos \beta}$$

where  $\alpha_0 < \alpha < \infty$ , and  $-\pi < \beta < \pi$  defines the region outside the cylinder. The geometric constants  $\alpha_0$  and  $c$  are defined as

$$\begin{aligned} \alpha_0 &= \text{sech}^{-1}(a/h) \\ c &= \frac{h}{\coth \alpha_0} \end{aligned}$$

(note that there is a typo in the expression for  $\alpha_0$  in [47]). The hydrodynamic and electrostatic forces on the cylinder are calculated to be

$$\begin{aligned} F_H &= \frac{2\pi \sinh \alpha_0 E_{\infty}^2 c}{(\alpha_0 \cosh \alpha_0 - \sinh \alpha_0) \coth \alpha_0} \times \left\{ \frac{1}{2 \sinh^2 \alpha_0} + \sum_{n=1}^{\infty} \left( \frac{\cosh \alpha_0}{\sinh(n+1)\alpha_0 \sinh \alpha_0} - \frac{1}{\sinh(n+2)\alpha_0 \sinh n\alpha_0} \right) \right\} \hat{\mathbf{y}} \\ F_E &= \frac{2\pi E_{\infty}^2 h}{\coth \alpha_0} \sum_{n=1}^{\infty} \left( \frac{n^2}{\sinh^2 n\alpha_0} - \frac{n(n+1) \cosh \alpha_0}{\sinh n\alpha_0 \sinh(n+1)\alpha_0} \right) \hat{\mathbf{y}} \end{aligned}$$

Because of symmetry, there is no force in the horizontal direction.

We are going to use this solution to gain some confidence in our numerical simulations. In Fig.3, you can see the comparison of COMSOL results with the analytical expression. The match is especially good when the particle is close to the wall. It gets worse as this distance increases, because the effects from the other walls also kick in. The simulation in Fig.3 has run with a box of size 20x20, and maximum mesh size 1, with finer mesh on the particle, specifically a maximum size of 0.1. Experimentation with Comsol shows that the hydrodynamic error is sensitive to the size of the box, while the error in the electrostatic force is more sensitive to

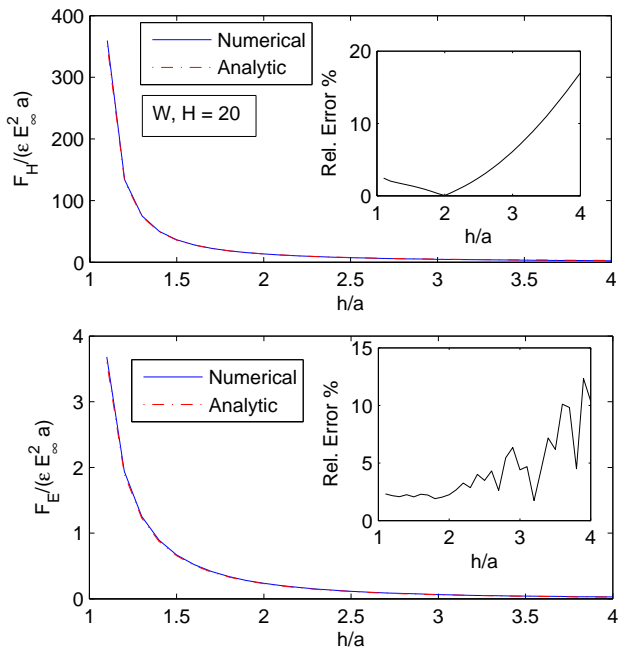


FIG. 3: The Comsol numerical solution is compared to the analytical one given by Zhao and Bau. Although the absolute errors tend to remain small, and the curves look identical, the relative error grows fast as the particle is located at larger distances from the planar wall.

the mesh size. For a larger box, 40x40, and twice as finer mesh, we have obtained a similar picture with errors cut to about one third of their values in Fig.3 (results not shown).

### B. Cylinder in an AC field

As the electric fields are screened quickly by the electrolyte, an AC field is usually preferred. Use of an AC electric field also prevents harmful reactions on electrodes, and enables experimentalists to go to higher applied voltage differences. Such higher voltages may be desirable if they lead to stronger electrokinetic effects of interest.

Far from the wall, the ICEO slip velocity around an ideally polarizable cylinder in an AC field was derived by Squires and Bazant [39], which takes the dimensionless form

$$\langle u_\theta \rangle = \frac{\sin 2\theta}{1 + \omega^2}. \quad (8)$$

We use this expression to calibrate our numerical code, and find excellent agreement far from the wall. This result shows that ICEO flow decays algebraically as  $\omega^{-2}$  above the RC charging frequency. Since electrostatic forces do not decay in this limit, we may expect a change in behavior near the wall. At high frequency, there is not enough time for double-layer

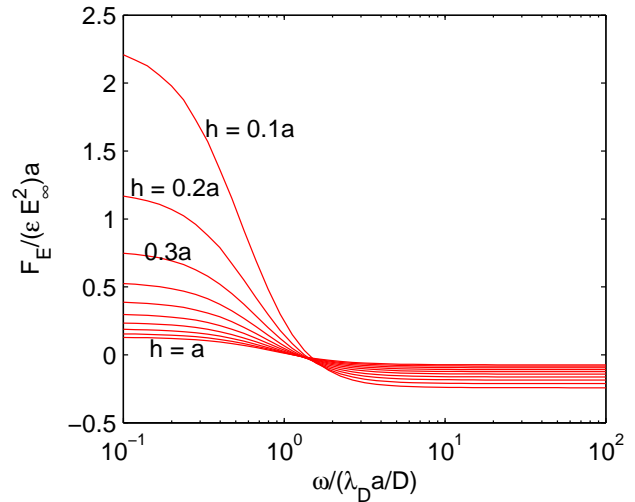


FIG. 4: The total electrostatic force on the cylinder changes sign as the frequency is increased. As the frequency approaches infinity, this force has a finite nonzero limit.

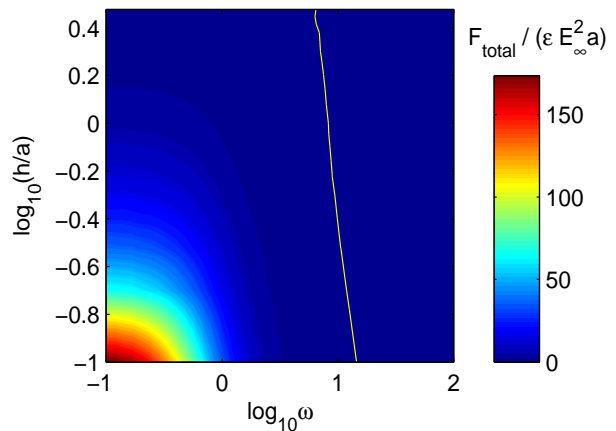


FIG. 5: Contour plot of total force on the ideally polarizable cylinder. There is an equilibrium distance between the cylinder and the wall at high enough frequencies, indicated by the yellow contour line. As the frequency is increased, this distance decreases.

relaxation, so the electric field resembles that of a conductor in a uniform dielectric medium.

An important observation is that the total hydrodynamic forces vanishes at higher frequencies whereas the total electrostatic force changes sign. As a result, if the frequency is high enough, there is an equilibrium distance from the wall. This distance decreases as the frequency is increased.

In the high frequency limit, the electrostatic problem approaches to the solution of the dirichlet problem, that is, the

laplace equation

$$\nabla^2 \tilde{\phi} = 0$$

combined with the boundary condition

$$\begin{aligned} \tilde{\phi} &= 0 \quad (\text{on the cylinder}) \\ n \cdot \nabla \tilde{\phi} &= 0 \quad (\text{on the wall}) \\ \tilde{\phi} &= -E_\infty x \quad (\text{at infinity}) \end{aligned}$$

In this case, the solution is given by

$$\phi = \text{Re}(\hat{\phi} e^{i\omega t}) = \hat{\phi} \cos \omega t$$

This problem can be solved analytically, and the solution is given by

$$\begin{aligned} \tilde{\phi} &= 2cE_\infty \sum_{n=1}^{\infty} \frac{e^{-n\alpha_0}}{\cosh n\alpha_0} \cosh n\alpha \sin n\beta - \frac{c \sin \beta}{\cosh \alpha - \cos \beta} \\ &= 2c \sum_{n=1}^{\infty} \left[ \frac{e^{-n\alpha_0}}{\cosh n\alpha_0} \cosh n\alpha - e^{-n\alpha} \right] \sin n\beta \end{aligned}$$

Plugging this into the electrostatic force leads to the formula

$$\begin{aligned} F_{E,\omega \rightarrow \infty} &= -2\pi c E_\infty \sum_{n=1}^{\infty} \left( \frac{n^2}{\cosh^2 n\alpha_0} \right. \\ &\quad \left. + \frac{n(n+1) \cosh \alpha_0}{\sinh n\alpha_0 \sinh(n+1)\alpha_0} \right) \end{aligned}$$

with the same notation as in Zhao and Bau.

### C. Sphere in an AC field

ICEO flow around a sphere was first considered by Gamayunov et al. [10]. Following the cylinder analysis of Squires and Bazant [39], it is straightforward to derive the (dimensionless) ICEO slip velocity around an ideally polarizable sphere in an AC field, far from the wall,

$$\langle u_\theta \rangle = \frac{9}{16} \frac{\sin 2\theta}{1 + (\omega/2)^2} \quad (9)$$

Note that since  $\langle \cos^2 \omega t \rangle = 1/2$  the ICEO flow in a constant DC field  $E_0$  is twice as large as the time-averaged flow in an AC field  $E_0 \cos \omega t$  of the same amplitude:  $u_\theta^{DC} = 2\langle u_\theta^{AC} \rangle$ .

For a sphere near a wall, the results are qualitatively the same as for a cylinder near a wall. That is, in the DC case, both the hydrodynamic and the electrostatic forces are repulsive. Moreover, the magnitude of hydrodynamic forces are about 2 orders of magnitude larger than the electrical forces.

Note that the steady and time-periodic plots are consistent: At  $h/a = 1.5$ , the steady plots show forces about  $F_H \approx 8$  and  $F_E \approx 0.12$ . The time-periodic plots, at the low

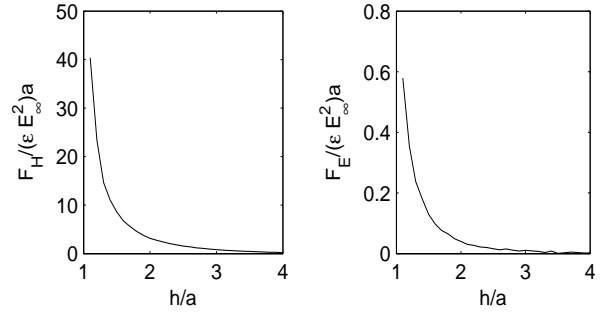


FIG. 6: The hydrodynamic and electrostatic forces on a full metal sphere.

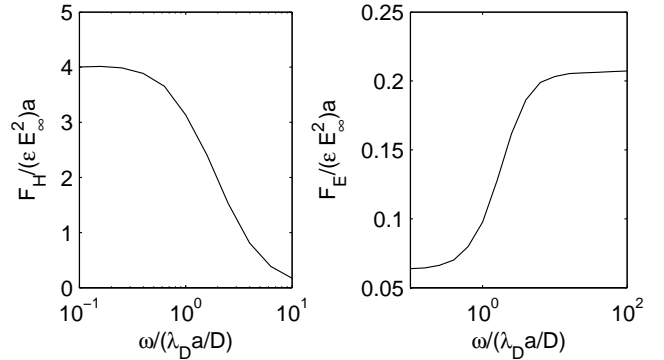


FIG. 7: Both the hydrodynamic and the electrostatic forces on an isotropic sphere are repulsive (away from the wall). While hydrodynamic forces on the sphere decline as a function of forcing frequency, electrostatic forces get stronger.

frequency limit, start off at values  $F_H \approx 4$  and  $F_E \approx 0.06$ , which are half of their steady counterparts.

Unlike the cylinder problem, however, the electrostatic forces always remain repulsive, and therefore there is no equilibrium plane for the spherical particle. Instead, it is repelled to infinity by the wall regardless of the forcing frequency.

## IV. JANUS SPHERE NEAR A WALL

### A. Broken symmetries

Without a nearby wall, a Janus sphere would align itself perpendicular to the electric field, that is, some of the electric field lines would be included in the plane dividing the Janus particles metal and insulating sides. This effect has been demonstrated in [40], and is presumably stronger than the wall effects, at least when the particle is sufficiently away from the wall. That being said, we will assume that the particle always stays in the described configuration, that is, its

dividing plane aligned with the electric field. This is not to say that the particle has no room for different rotational configurations, it can still rotate around  $x$  and  $y$  axis. Rotations about the  $y$ -axis (if existed) leave the particle unchanged, so we are left with rotations only around the  $x$ -axis. This is much easier to deal with than the original problem though, as only one angle is enough to describe the particle's orientation.

Far from the wall, the bulk velocity perpendicular to a DC field in the stable orientation is given by the formula of Squires and Bazant [40] (Eq. 3.16), which takes the dimensionless form,

$$U_{DC} = \frac{9}{64} = 2\langle U_{AC}(\omega \rightarrow 0) \rangle \quad (10)$$

neglecting compact-layer surface capacitance. As noted above, the time-averaged velocity in a sinusoidal AC field is smaller by a factor of two in the limit of zero frequency. Even in the bulk, without a wall, it is difficult to solve analytically for the ICEO flow at finite AC frequency around a Janus particle, since the electrical response is not simply an induced dipole, due to the broken symmetry. Nevertheless, we will see that the frequency dependence of the flow is similar to that around a sphere (9), constant below the RC charging time and decaying above it.

For a Janus sphere aligned perpendicular to the electric field near a wall, a crucial observation is that the  $y$ -symmetry breaks down. As a result, there is a net force in the  $y$ -direction, as well as a net torque in  $x$ -direction. The former leads to translation parallel to the wall, while the latter causes rotation of the dielectric face toward the wall. We shall see that these effects of broken symmetry completely change the behavior near wall in an AC or DC field: Although a polarizable sphere is always repelled to infinity by an insulating wall, a Janus particle is always (eventually) attracted to it.

### B. Basic mechanism for wall attraction

The key new effect is rotation due to hydrodynamic torque caused by asymmetric ICEO flow near the wall. This generally causes the Janus particle to be attracted to the wall, as shown in figure 8. The physical mechanism can be understood as follows. When the field is first turned on, the Janus particle quickly rotates, by ICEP and DEP, to align its metal/insulator interface with the field axis, but with an arbitrary azimuthal angle, mainly set by the initial condition. As described by Squires and Bazant [40], the ICEO flow around the particle draws in fluid along the field axis and ejects it radially at the equator – but only on the polarizable hemisphere, which acts like a “jet engine” drives ICEP motion in the direction of the non-polarizable hemisphere, which leads the way like a “nose”.

Near a wall, as shown in the figure, the outward ICEO flow pushes down on the wall harder on the side of the polarizable

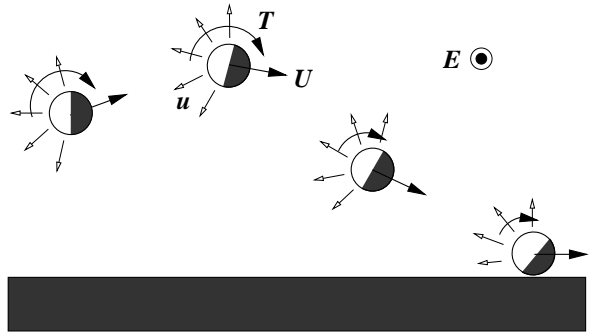


FIG. 8: Sketch of ICEO flows  $u$  and resulting ICEP torques  $T$  which cause a Janus particle to tilt its less polarizable end toward a wall, while translating toward the wall (until stopped by double-layer overlap) and perpendicular to the applied AC field  $E$  (directed into the page and parallel to the wall). This physical mechanism may explain why the transverse ICEP motion of Janus particles was observable over the surface of a glass wall in the experiments of Gangwal et al. [11].

“engine” than on that of the non-polarizable “nose”, which produces a hydrodynamic torque tilting the nose toward the wall. A second cause of this rotation is the hydrodynamic coupling between ICEP translation parallel to the wall and rotation by shear stresses to cause rolling past the wall. Regardless of the initial position, these two sources of ICEP rotation cause the nose to eventually face the wall, so that the translational engine drives it toward the wall. This is likely the origin of the counter-intuitive attraction of Janus particles to a glass wall in the experiments of Gangwal et al [11].

What happens next depends on the details of the particle-wall interaction at very close distances. We will see that the bulk model with thin double layers must eventually break down, since the particle eventually collides with the wall, leading to overlapping particle and wall double layers. It is beyond the scope of this work to accurately treat the nonlinear and time-dependent behavior of these overlapping double layers, so we will explore two models: (i) infinitely thin double layers, i.e. using the bulk model to arbitrarily small heights, and (ii) a cutoff “collision” height, where overlapping double layers stop any further motion toward the wall, while still allowing transverse motion. The latter case assumes, as in the experiments [11], that the particles and walls have *equilibrium* surface charge of the same sign. For concreteness, we will simulate Model (ii) with a cutoff height  $h = \lambda = 0.05a$ , e.g. corresponding to a double-layer thickness (screening length) of  $\lambda = 50\text{nm}$  with particles of size  $a = 1\mu\text{m}$ .

Based on the simple examples above, we expect a subtle dependence on the AC frequency. Electrostatic DEP motion will always begin to dominate the hydrodynamic ICEP motion at high frequency. Therefore, we now consider the low and high frequency cases separately.

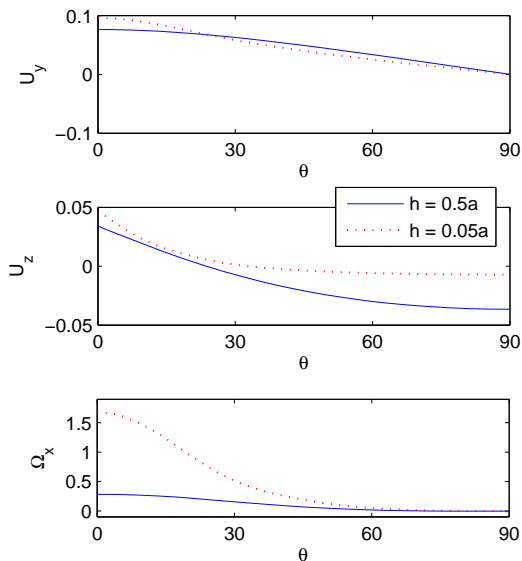


FIG. 9: In the DC limit ( $\omega \rightarrow 0$ ), we plot (a) horizontal velocity (b) vertical velocity and (c) tilting speed (degrees/charging time) as a function of the tilt angle  $\theta$  for the janus particle at distances  $h = 0.5a$  and  $h = 0.05a$  from the wall.

### C. Dynamics as a function of AC frequency

As shown in Fig. 9, in the low frequency limit, the Janus particle experiences a rotational velocity turning its non-polarizable side toward the wall, as explained above. The hydrodynamic ICEP torque is orders of magnitude larger than the electrostatic DEP torque, until the particle gets quite close to the wall. The magnitude of the horizontal ICEP velocity  $U_y$  parallel to the surface and perpendicular to the field is close to its bulk value  $U_y = 9/128 \approx 0.07$  even fairly close to the wall at a height  $h = 0.5a$  at zero tilt, but reduces with the tilt angle. For small tilt angles and close to the wall at  $h = 0.05a$ , the horizontal velocity increases to  $U_y \approx 0.10$ , but it drops below the bulk value at larger tilt angles, e.g. to  $U_y \approx 0.05$  at  $\theta = 45$  degrees. Below we will see that this velocity is further reduced at higher forcing frequencies, due to the reduction of ICEO flow (since DEP cannot contribute to motion perpendicular to a uniform field).

Regardless of the orientation, in the DC limit the particle moves ever closer to the wall in Model (i) since  $U_z < 0$  for any tilting of the nose toward the wall. Even if the vertical motion is stopped at a critical height in Model (ii), the rotation continues in the DC limit until the particle points its non-polarizable nose directly at the wall ( $\theta = 90$ ) and the motion stops, although this can take a long time, since the rotation slows down substantially for tilt angles larger than 45 degrees. As discussed below, a number of effects might lead to such a stabilization of the tilt angle, thus allowing

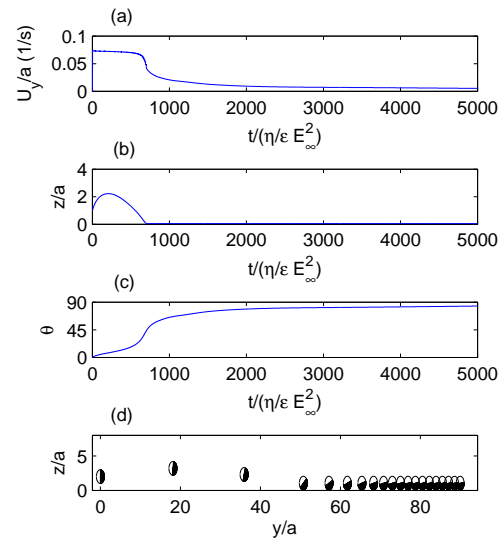


FIG. 10: Typical trajectory of a janus particle under the DC limit  $\omega \rightarrow 0$  interacting with the wall: As a function of time, plotted are (a) The horizontal speed (b) Distance from the wall (c) Tilt angle. Also, we plot the distance from the wall as a function of horizontal position in (d).

steady translation along the wall.

As shown in Fig. 10, a typical simulated trajectory of the Janus particle shows it translating perpendicular to the field while rotating and attracting to the wall, until eventually coming to rest facing the wall. Even when the particle's motion stops, however, its polarizable hemisphere (“engine”) continues driving a steady ICEO flow, which can lead to long-range hydrodynamic interactions with other particles. This is an interesting theoretical prediction which should be checked in experiments. Such immobilized Janus particles may have interesting applications in microfluidics.

Similar behavior is predicted for finite AC frequencies in many cases. In particular, if a particle is initially mostly facing its non-polarizable hemisphere toward the wall ( $\theta$  near  $90^\circ$ ), it will swim toward the wall and come to rest, as in the DC limit of Figure 10.

There are some new effects in AC fields, however, since ICEO flows are suppressed with increasing frequency. The competing effect of DEP can prevent the Janus particle from fully rotating and coming to rest on the surface, at least in Model (ii) where the collision is prevented artificially, as shown in Figure 12. At  $\omega = 1$  (the characteristic RC frequency of the particle), the rotation slows down substantially beyond  $45^\circ$  but does not appear to stop. In this regime the horizontal velocity decays to  $U_y \approx 0.015$ . For  $\omega = 10$  the particle appears to settle down to an equilibrium tilt angle around  $45^\circ$ , while steadily translating over the wall. The limiting horizontal velocity is roughly  $U_y \approx 0.009$ .

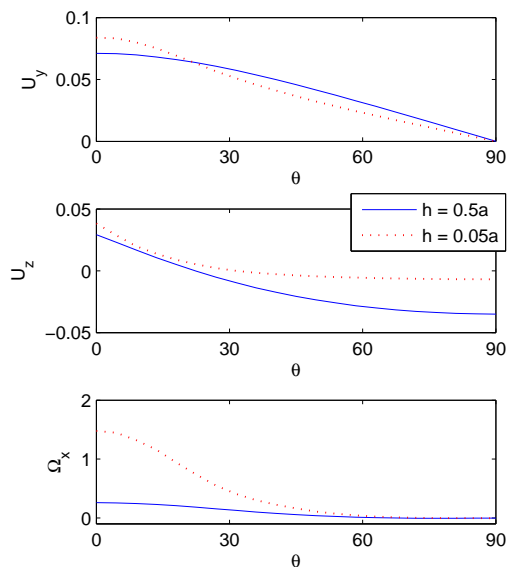


FIG. 11: For AC frequency  $\omega\tau_c = 1$ , we plot (a) horizontal velocity (b) vertical velocity and (c) tilting speed (degrees/charging time) as a function of the tilt angle  $\theta$  for the janus particle at distances  $h = 0.5a$  and  $h = 0.05a$  from the wall.

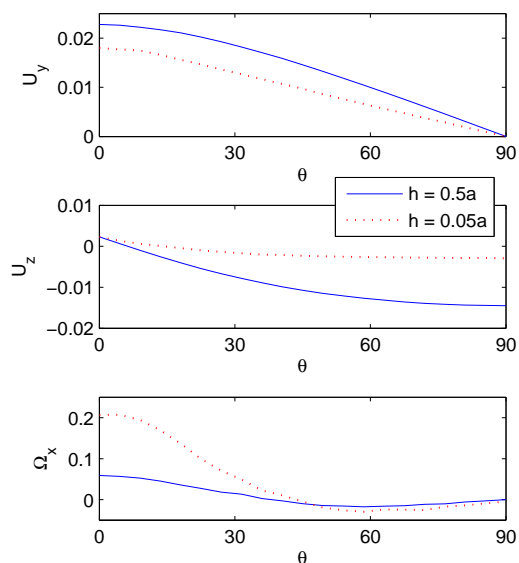


FIG. 13: For AC frequency ( $\omega\tau_c = 10$ ), we plot (a) horizontal velocity (b) vertical velocity and (c) tilting speed (degrees/charging time) as a function of the tilt angle  $\theta$  for the janus particle at distances  $h = 0.5a$  and  $h = 0.05a$  from the wall.

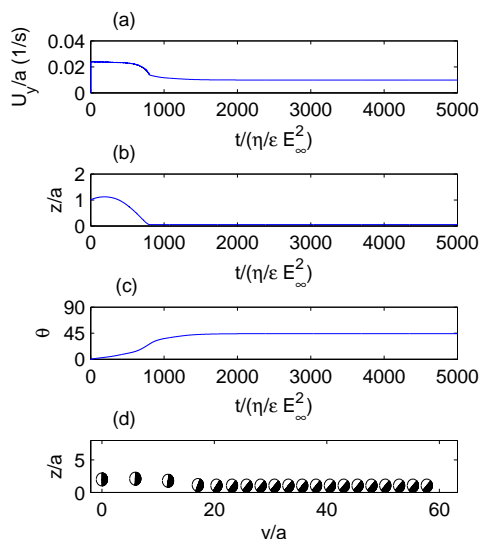


FIG. 12: Typical trajectory of a janus particle under AC frequency  $\omega\tau_c = 10$  interacting with the wall: As a function of time, plotted are (a) The horizontal speed (b) Distance from the wall (c) Tilt angle. Also, we plot the distance from the wall as a function of horizontal position in (d).

#### D. Comparison to experiment

The simulations with Model (ii) are in reasonable agreement with the experimental observations of Gangwal et al [11] for metallo-dielectric Janus particles in dilute NaCl solutions in the low-frequency regime  $\omega < 1$ . The bulk theory of Squires and Bazant (10) accurately fits the experimental velocity as a function of the field strength (Fig. 3 of Ref. [11]) and the particle size (Fig. 4), if a ratio  $\delta = 10$  for the compact-layer to diffuse-layer capacitance is used to obtain the dimensionless formula,  $U_{expt} = (9/128)/(1+10) = 0.006$ . However, the ICEP motion is observed only very close to the walls.

Our simulations predict that the particles are quickly attracted to the walls over a time of order the channel width ( $60 \mu\text{m}$ ) divided by the typical ICEP velocity ( $10 \mu\text{m/s}$ ), which is roughly one minute, consistent with experimental observations. The particles are also predicted to tilt, and moderate tilt angles can also be inferred from experimental images, although more accurate measurements are needed. If the tilt angle stabilizes around  $45^\circ$  (see below), then the simulations (Fig. 9) predict that the ICEP translational velocity should be only  $0.05/0.07 = 70\%$  of the bulk value close to the wall, which would imply  $\delta = 7$ . This value is somewhat larger than that inferred from prior experiments on ICEO flow in dilute KCl around a larger ( $100 \mu\text{m}$  radius) platinum cylinder [23], but it is also observed that the ICEP velocity is slower than predicted at larger sizes (Fig. 4 of Ref. [11]).

Apart from the rotational dynamics, therefore, the theory is able to predict the ICEP velocity fairly well.

Without stopping the rotation artificially, we are able to predict the experimentally observed steady motion along the wall only at moderate to large  $\omega$ . The reduction of ICEO flow in this regime reduces hydrodynamic torque (see below) and also enhances the effect of stabilizing electrostatic forces. Although  $U_{expt} = 0.006$  is measured in the low-frequency plateau  $\omega < 1$ , this behavior otherwise seems quite consistent, since the slower ICEP velocity can also fit the experimental data using smaller (and perhaps more reasonable) values of  $\delta$ . For example, the predicted velocity of  $U = 0.015$  at  $\omega = 1$  implies  $\delta = 1.5$ , while the velocity  $U = 0.009$  at  $\omega = 10$  implies  $\delta = 0.5$ .

The difficulty in predicting the stable tilt angle at low frequency may be due to our use of the low-voltage, dilute-solution theory, which generally overpredicts the magnitude of ICEO flows, especially with increasing salt concentration. For example, the electrophoretic mobility can saturate at large induced voltages, and the charging dynamics can also be altered significantly when crowding effects are taken into account [5]. As a result, our simulation results at moderate frequencies  $\omega = 1 - 10$ , which exhibit reduced ICEO flow due to incomplete double-layer charging, may resemble the predictions of more accurate large-voltage, concentrated-solution theories at low frequency  $\omega < 1$ , where flow is reduced instead by ion crowding in the double layer. This will be the subject of future work.

### E. Contact mechanics

Another source of error in the model is our inaccurate treatment of the contact region, where double-layers overlap. We have simply imposed a small cutoff height in Model (ii) to prevent the wall collision, but there may be more complicated mechanical effects of the contact region. In particular, there may be enhanced hydrodynamic slip, due to the repulsion of overlapping (equilibrium) double layers of the same sign, as in the experiments.

By examining the forces and torques close to the wall, we can infer to some degree what mechanical properties of the contact region might lead to the observed ICEP sliding along the wall and smaller tilt angles at lower frequencies (and thus also somewhat larger velocities). As shown in Fig. 14, before the particle gets very close to the wall, the (mostly hydrodynamic) torque acts to completely tilt the non-polarizable face toward the wall leading to collision. As noted above in Fig. 8, this can be understood as a result of the downward component of ICEO flow on the polarizable hemisphere raising the pressure by pushing on the wall on that side.

The situation changes when the particle gets very close to the wall. As shown in Fig. 14, the torque changes sign at a tilt angle which is roughly  $45^\circ$ . This again can be understood from Fig. 8, since the ICEO flow between the particle and the wall on the polarizable side, which drives the

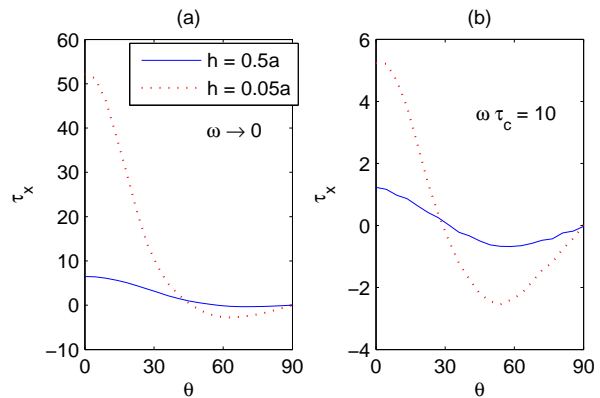


FIG. 14: Torque on a fixed Janus sphere versus tilt angle at heights  $h = 0.5a$  and  $0.05a$  when (a)  $\omega \rightarrow 0$  (b)  $\omega\tau_c = 10$ .

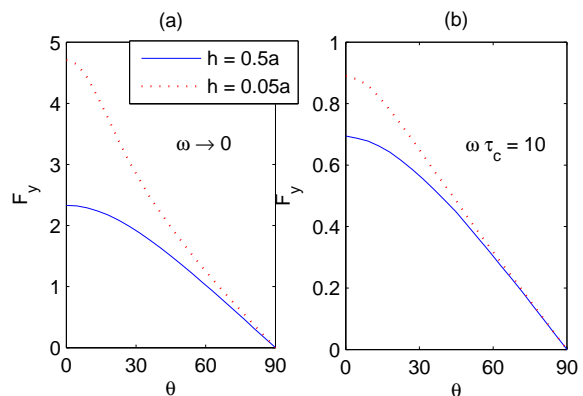


FIG. 15: Horizontal force on a fixed Janus sphere versus tilt angle at heights  $h = 0.5a$  and  $0.05a$  when (a)  $\omega \rightarrow 0$  (b)  $\omega\tau_c = 10$ .

torque, is mostly absent. It would thus seem that even in a DC field, the particle would not rotate any farther, but this thinking neglects the hydrodynamic coupling between translational force and rotational velocity near the wall, Eq. (4). In Fig. 15, we see that the force on the particle parallel to the wall  $F_y$  remains strong, and this leads to a rolling effect over the wall due to shear stresses. For this reason, the rotational velocity persists in Fig. 9 even when the torque goes to zero in Fig. 14.

The model assumes no slip on all non-polarizable surfaces, but this may not be a good approximation near the contact point when double layers overlap. If the equilibrium surface charges (or zeta potentials) on the non-polarizable hemisphere and the wall have opposite signs, then the overlapping double layers lead to a strong attraction, which would only stiffen the effective contact with the surface, and thus only increase the viscous rolling effect during motion along the surface. If the equilibrium surface charges (or zeta potentials) have the same sign, however, as in the experiments on

gold-coated latex Janus particles near glass walls [11], then there is a strong repulsion at the contact point. This repulsion stops the collision with the wall in Model (ii), but it may also “lubricate” the contact and allow for some sliding. This effective slip over the wall near the contact point could reduce the viscous rolling, and, in the absence of torque, cause the rotation to stop, or at least be reduced for tilt angles above  $45^\circ$ . In that case, we might expect a more accurate model of the contact region to predict to the experimentally observed motion, sliding over the surface by ICEP with a small tilt angle ( $\theta < 45^\circ$ ), for a wider range of conditions, including lower AC frequency, perhaps even in the DC limit.

## V. CONCLUSION

We have used the existing low-voltage theory of ICEP to predict the motion of polarizable particles near an insulating wall. Our results for symmetric spheres and cylinders confirm the expected repulsion from the wall due to ICEO flow, sketched in Figure 1(a). In the case of the cylinder we show that attraction is also possible at high frequency, where DEP from electrostatic forces dominates slip-driven ICEP motion.

Our results for asymmetric Janus particles reveal an unexpected attraction to the wall by a novel mechanism illustrated in Figure 8, which involves tilting of the less polarizable face toward the wall. Once it reaches the wall, if double-layer repulsion prevents further collision, the particle either rotates completely and ceases to move, while driving steady ICEO flow, or reaches an equilibrium tilt angle around  $45^\circ$  while steadily translating along the surface, perpendicular to the electric field. The latter motion only arises at moderate frequencies in our model, above the characteristic charging frequency for the double layers, while in experiments it is also observed at low frequencies. More accurate models taking into account reduced ICEO flow at large voltage in non-dilute solutions and more accurate models of the contact region may improve the agreement with experiments.

In any case, we have shown that polarizable particles can display complex interactions with walls due to broken symmetries in ICEO flows. Attractive and repulsive interactions can be tuned by varying the geometry of the particles (and the walls), as well as the AC frequency and voltage. These phenomena may find applications in separations and self-assembly of colloids or in local flow generation in microfluidic devices.

- 
- [1] J. L. Anderson. Effect of non-uniform zeta potential on particle movement in electric fields. *J. Colloid Interface Science*, 105:45–54, 1984.
  - [2] J. L. Anderson. Colloid transport by interfacial forces. *Annu. Rev. Fluid Mech.*, 21:61–99, 1989.
  - [3] M. Z. Bazant. Electrokinetic motion of polarizable particles. In Dongqing Li, editor, *Encyclopedia of Microfluidics and Nanofluidics*. Springer, 2008.
  - [4] M. Z. Bazant and T. M. Squires. Induced-charge electrokinetic phenomena: Theory and microfluidic applications. *Phys. Rev. Lett.*, 92:066101, 2004.
  - [5] Martin Z. Bazant, Mustafa Sabri Kilic, Brian Story, and Armand Ajdari. Nonlinear electrokinetics at large voltages. arXiv:cond-mat/0703035v2.
  - [6] M.-H. Chih and J.-P. Hsu. Electrophoresis of a sphere normal to a plane at arbitrary electrical potential and double layer thickness. *J. Colloid Interface Science*, 248:383–388, 2002.
  - [7] S. M. Davison and K. V. Sharp. Boundary effects on the electrophoretic motion of cylindrical particles: Concentrically and eccentrically positioned particles in a capillary. *J. Colloid Interface Science*, 303:288–297, 2006.
  - [8] J. Ennis and J. L. Anderson. Boundary effects on electrophoretic motion of spherical particles for thick double layers and low zeta potential. *J. Colloid Interface Science*, 185:497–514, 1997.
  - [9] M. C. Fair and J. L. Anderson. Electrophoresis of heterogeneous colloids – doublets of dissimilar particles. *Langmuir*, 8:2850–2854, 1992.
  - [10] N. I. Gamayunov, V. A. Murtsovkin, and A. S. Dukhin. Pair interaction of particles in electric field. 1. features of hydrodynamic interaction of polarized particles. *Colloid J. USSR*, 48:197–203, 1986.
  - [11] S. Gangwal, O. J. Cayre, M. Z. Bazant, and O. D. Velev. Induced-charge electrophoresis of metallo-dielectric particles. arXiv:0708.2417v1, 2007.
  - [12] K. D. Horng H. J. Keh and J. Kuo. Boundary effects on electrophoresis of colloidal cylinders. *J. Fluid Mech.*, 231:211–228, 1991.
  - [13] J.-P. Hsu, Z.-S. Chen, M.-H. Ku, and L.-H. Yeh. Effect of charged boundary on electrophoresis: Sphere in a spherical cavity at arbitrary potential and double-layer thickness. *J. Colloid Interface Sci.*, 314:256–263, 2007.
  - [14] J.-P. Hsu and M.-H. Ku. Boundary effect on electrophoresis: finite cylinder in a cylindrical pore. *J. Colloid Interface Sci.*, 283:592–600, 2005.
  - [15] J.-P. Hsu, L.-H. Yeh, and Z.-S. Chen. Effect of a charged boundary on electrophoresis: A sphere at an arbitrary position in a spherical cavity. *J. Colloid Interface Sci.*, 310:281–291, 2007.
  - [16] J.-P. Hsu, L.-H. Yeh, and M.-H. Ku. Evaluation of the electric force in electrophoresis. *J. Colloid Interface Sci.*, 305:324–329, 2007.
  - [17] R. J. Hunter. *Foundations of Colloid Science*. Oxford University Press, Oxford, 2001.
  - [18] H. J. Keh and J. L. Anderson. Boundary effects on the electrophoretic motion of colloidal spheres. *J. Fluid Mech.*, 153:417–439, 1985.
  - [19] H. J. Keh and S. B. Chen. Electrophoresis of a colloidal sphere parallel to a dielectric plane. *J. Fluid Mech.*, 194:377–390, 1988.
  - [20] H. J. Keh and J. S. Jan. Boundary effects on diffusiophoresis and electrophoresis: Motion of a colloidal sphere normal to a plane wall. *J. Colloid Interface Science*, 183:458–475, 1996.

- [21] E. Lee, J.-W. Chu, and J.-P. Hsu. Electrophoretic mobility of a spherical particle in a spherical cavity. *J. Colloid Interface Science*, 196:316–320, 1997.
- [22] Eric Lee, Jih-Wei Chu, and Jyh-Ping Hsu. Electrophoretic mobility of a sphere in a spherical cavity. *J. Colloid Interface Science*, 205:65–76, 1998.
- [23] J. A. Levitan, S. Devasenathipathy, V. Studer, Y. Ben, T. Thorsen, T. M. Squires, and M. Z. Bazant. Experimental observation of induced-charge electro-osmosis around a metal wire in a microchannel. *Colloids and Surfaces A*, 267:122–132, 2005.
- [24] Hui Liu, Haim H. Bau, and Howard H. Hu. Electrophoresis of concentrically and eccentrically positioned cylindrical particles in a long tube. *Langmuir*, 20:2628–2639, 2004.
- [25] D. Long and A. Ajdari. Electrophoretic mobility of composite objects in free solution: Application to dna separation. *Electrophoresis*, 17:1161–1166, 1996.
- [26] D. Long and A. Ajdari. Symmetry properties of the electrophoretic motion of patterned colloidal particles. *Phys. Rev. Lett.*, 81:1529–1532, 1998.
- [27] J. Lyklema. *Fundamentals of Interface and Colloid Science. Volume II: Solid-Liquid Interfaces*. Academic Press Limited, San Diego, CA, 1995.
- [28] F. A. Morrison and J. J. Stukel. Electrophoresis of an insulating sphere normal to a conducting plane. *J. Colloid and Interface Science*, 33:88, 1970.
- [29] V. A. Mursovkin and G. I. Mantrov. Study of the motion of anisometric particles in a uniform variable electric field. *Colloid J. USSR*, 52:933–936, 1990.
- [30] V. A. Mursovkin. Nonlinear flows near polarized disperse particles. *Colloid Journal*, 58:341–349, 1996.
- [31] G. C. Randall and P. S. Doyle. Dna deformation in electric fields: Dna driven past a cylindrical obstruction. *Macromolecules*, 38:2410–2418, 2005.
- [32] W. D. Ristenpart, I. A. Aksay, and D. A. Saville. Electrically guided assembly of planar superlattices in binary colloidal suspensions. *Phys. Rev. Lett.*, 90, 2003.
- [33] W. D. Ristenpart, I. A. Aksay, and D. A. Saville. Ehd flow around a colloidal particle near an electrode with an oscillating potential. *J. Fluid Mech.*, 575, 2007.
- [34] Klint Rose and Juan G. Santiago. Rotational electrophoresis of striped metallic microrods. *Physical Review E*, 75:197–203, 2006.
- [35] W. B. Russel, D. Saville, and W. R. Schowalter. *Colloidal Dispersions*. Cambridge University Press, Cambridge, England, 1989.
- [36] D. Saintillan, E. Darve, and E. S. G. Shaqfeh. Hydrodynamic interactions in the induced-charge electrophoresis of colloidal rod dispersions. *Journal of Fluid Mechanics*, 563:223–259, 2006.
- [37] Alexander A. Shugai and Steven L. Carnie. Electrophoretic motion of a spherical particle with a thick double layer in bounded flows. *J. Colloid Interface Science*, 213:298–315, 1999.
- [38] Paul J. Sides. Electrohydrodynamic particle aggregation on an electrode driven by an alternating electric field normal to it. *Langmuir*, 17:5791–5800, 2001.
- [39] T. M. Squires and M. Z. Bazant. Induced-charge electro-osmosis. *J. Fluid Mech.*, 509:217–252, 2004.
- [40] T. M. Squires and M. Z. Bazant. Breaking symmetries in induced-charge electro-osmosis and electrophoresis. *J. Fluid Mech.*, 560:65–101, 2006.
- [41] T. M. Squires and S. R. Quake. Microfluidics: fluid physics on the nanoliter scale. *Rev. Mod. Phys.*, 77, 2005.
- [42] Y.-P. Tang, M.-H. Chih, Eric Lee, and J.-P. Hsu. Electrophoretic motion of a charge-regulated sphere normal to a plane. *J. Colloid Interface Sci.*, 242:121–126, 2001.
- [43] M. Trau, D. A. Saville, and I. A. Aksay. Assembly of colloidal crystals at electrode interfaces. *Langmuir*, 13:6375, 1997.
- [44] E. Yariv. Induced-charge electrophoresis of nonspherical particles. *Phys. Fluids*, 17:051702, 2005.
- [45] Ehud Yariv. Force-free electrophoresis? *Phys. Fluids*, 18:031702, 2006.
- [46] S. Yeh, M. Seul, and B. Shraiman. Assembly of ordered colloidal aggregates by electric-field-induced fluid flow. *Nature (London)*, 386:57, 1997.
- [47] H. Zhao and H. H. Bau. On the effect of induced electro-osmosis on a cylindrical particle next to a surface. *Langmuir*, 23:4053–4063, 2007.
- [48] Andrew L. Zydney. Boundary effects on electrophoretic motion of a charged particle in a spherical cavity. *J. Colloid Interface Science*, 169:476–485, 1995.

